# Analysis of the Temperature-Dependent Phonon Structure in Sodium Nitrite by Raman Spectroscopy*

C. M. Hartwig,† E. Wiener-Avnear,‡ and S. P. S. Porto
*Departments of Physics and Electrical Engineering, University of Southern California, Los Angeles, California* 90007
(Received 19 July 1971)

The temperature behavior of the TO-phonon frequencies and line shapes in $NaNO_2$, as observed by Raman spectroscopy, is reported for temperatures from 20 to 250 °C. The Raman spectra of the ferroelectric phase obeyed the selection rules of the $C_{2V}^{20}$ space group. In the paraelectric Raman spectra, extra resonances (six instead of the expected three) were found. This anomaly and accompanying line asymmetries are accounted for by recognizing the effect of the nitrite-ion disordering along the *b* axis upon lattice states. Additionally, in the paraelectric Raman spectra [polarized and (*bc*)], a redundant appearance of the symmetric internal vibrations was observed, from which we conclude that above the phase-transition temperature there is a large torsional oscillation of the $NO_2^-$ ion about the *a* axis. Significantly, the librational frequency associated with this torsional oscillation softened at key temperatures, the temperatures at which long- and short-range orders are lost. From our data, we conclude that the nitrogen atom jumps between two equivalent lattice sites by the flipping of the nitrite ion about the *a* axis, and we suggest that temperature-dependent coupling between normal modes precipitates this flipping. A careful search of the Raman spectra 3 $cm^{-1}$ from the frequency of the incident laser revealed no "Cochran" soft modes or supernumerary modes, such as a dipole wave, that might explain the ferroelectric phase transition in $NaNO_2$.

## I. INTRODUCTION

In recent years, progress has been made in relating the phase transition in displacive ferroelectrics (i.e., $BaTiO_3$,[1] $SrTiO_3$,[2] etc.) to a softening of an optical transverse mode (proposed by Cochran[3]), as a ferroelectric phase-transition temperature is approached. The possibility that a soft-mode theory explains order-disorder ferroelectric transitions is controversial, and little experimental evidence has been found to justify this conjecture. In a simplified approach,[4] the ferroelectric transition in $NaNO_2$ is an order-disorder phase transition, marking sodium nitrite as an object for analysis in respect to order-disorder soft modes as well as other transition mechanisms. It is the paraelectric phase of $NaNO_2$ that is disordered. The nitrogen atom of the $NO_2^-$ ion appears to randomly jump to either the "left" or the "right" of the *ac* crystallographic plane.[5,6] This constitutes a twofold directional disordering of the intrinsic $NO_2^-$ dipole, which parallels the bisector of the O—N—O angle and points to its vertex. In the ferroelectric phase, which is the ordered phase, there is an ordered unidirectional alignment of the $NO_2^-$ dipole, accompanied by a displacement of the $Na^+$ ions along the *b* axis.

Sodium nitrite has excited extensive scientific investigation, since the discovery of its phase transition by Sawada *et al.* in 1958.[4] An incentive to perform research upon $NaNO_2$ has been the simple crystalline structures of the ferroelectric and paraelectric phases. Understanding the ferroelectric phase transition in $NaNO_2$ should lead to unraveling more complicated transitions. There have been numerous studies of the spontaneous polarization and dielectric constants.[4,7–10] An infrared analysis of sodium nitrite at room temperature has been done by Axe.[11] In addition, infrared experiments by Sato *et al.*,[12] Vogt *et al.*,[13] and Barnoski and Ballantyne[14] have provided useful temperature-dependent information about lattice states. Recent discussion of room-temperature Raman spectra may be found in articles by Tsuboi *et al.* and Hartwig *et al.*[16] There has been temperature-dependent analysis of $NaNO_2$ with Raman spectroscopy by Chisler and Shur[17] and Gorelik *et al.*[18]

The research reported in this paper supplements previous studies of $NaNO_2$ and extends the Raman survey of the crystal by a comprehensive Raman investigation of the temperature-dependent resonant frequencies of all the normal modes, an analysis of the temperature-dependent phonon line shapes, and an interpretation of the temperature-dependent Raman selection rules. We have found that the Raman spectra of the ferroelectric phase can be explained with the space symmetry group $C_{2V}^{20}$[19] for $NaNO_2$. However, if the $D_{2h}^{25}$ space-group symmetry[20] were used to explain the Raman spectra of the paraelectric phase, there were startling discrepancies. We point out that understanding of the paraelectric Raman spectra must incorporate the invalidity of the selection rules constructed from the $D_{2h}^{25}$ symmetry, because both the crystal's disorder and a significantly large oscillation of the nitrite anion in the *bc* crystal plane introduce spectral

violations.

In our research we have also focused upon understanding the mechanisms associated with the jumping of the nitrogen atom between equivalent lattice sites and the movement of the $Na^+$ ion, both of which establish the paraelectric phase. Specifically, we looked for soft modes and additional low-frequency structures ($< 10$ cm$^{-1}$) that might indicate the presence of supernumerary modes, such as vibrational tunneling, rotational tunneling, or a collective dipole wave (a mode similar to spin waves in magnetic crystals). Pertinent to the phase-transition mechanism in sodium nitrite, we have uncovered an inferred coupling between translational and librational phonons, a potential barrier decrease for the rotation about the $a$ axis, and an unusually large torsional oscillation of the nitrite ion about the $a$ axis in the paraelectric phase. From this, we conclude that the jumping of the nitrogen atom, which contributes to the phase transition and accounts for the disorder in the paraelectric phase, occurs by the flipping of the nitrite ion about the $a$ crystallographic axis.

## II. CRYSTAL STRUCTURE AND LATTICE DYNAMICS

At room temperature, the Bravais lattice of $NaNO_2$ (Fig. 1) determined by x-ray studies[19,21] is body-centered orthorhombic ($C_{2V}^{20}$ space symmetry) with one formula unit per primitive cell. The spontaneous polarization (parallel to the $b$ axis) has two contributors: the unit-cell dipole moment, established by the positions of the $Na^+$ cation and the $NO_2^-$ anion in the unit cell, and the intrinsic dipole moment of the $NO_2^-$ anion.

The transition from the ferroelectric phase in $NaNO_2$ to the upper-temperature nonpolar disordered phase is complicated, occurring in two steps at atmospheric pressure: the Curie temperature, $T_C = 163\,^\circ$C, and the Néel temperature, $T_N = 164\,^\circ$C.[22-24] Above $T_C$ a ferrielectric (antiferroelectric) sinusoidal modulation of the average dipole moment appears in the $a$ crystallographic direction. At temperatures above $T_N$ the crystal is paraelectric, gaining a statistical mirror plane $ac$. The nitrite ion can now point in either direction along the $b$ axis, and the sodium ion has centered itself on the unit-cell edge parallel to the $b$ axis.[5,20] X-ray analysis has assigned an orthorhombic space-group symmetry, $D_{2h}^{25}$,[5,20] (Fig. 1) to this nonpolar phase, which describes the crystal until the melting point at $T_M = 271\,^\circ$C. Again, there is one molecule in the primitive cell.

The narrow temperature phase between $T_C$ and $T_N$ was not studied by this research because the temperature resolution of the equipment was $\pm 0.75\,^\circ$C. Therefore, the phase-transition temperature discussed in the paper is that of the combined transition.

The primitive cell of sodium nitrite in both phases contains four atoms. Thus, the lattice modes have nine optical and three acoustical branches. In the ferroelectric phase, the optical modes have the following irreducible species[25,26]:

$$3A_1(aa,\ bb,\ cc):b + 1A_2(ac) + 3B_1(bc):c + 2B_2(ab):a\ . \quad (1)$$

The $a$, $b$, and $c$ refer to the conventional $NaNO_2$ biaxial axes (Fig. 1). The Raman tensor elements are given inside the parentheses in short notation, and the polarization direction of the polar modes is indicated by the letter behind the colon. Eight modes in the ferroelectric phase are both Raman and infrared active, and a TO-LO splitting is expected. At temperatures above $T_N$, the $D_{2h}^{25}$ space symmetry of the nonpolar phase implies that the optical normal modes separate into the following irreducible representations[25,26]:

$$1A_g(aa,\ bb,\ cc) + 1B_{1g}(ac) + 1B_{2g}(bc) + 2B_{1u}:b + 2B_{2u}:a + 2B_{3u}:c\ . \quad (2)$$

The $D_{2h}^{25}$ space symmetry group has a center of symmetry, preventing any simultaneous Raman and infrared activity. The disappearance of six lines from the Raman and two from the infrared spectra are therefore anticipated when the crystal's tem-

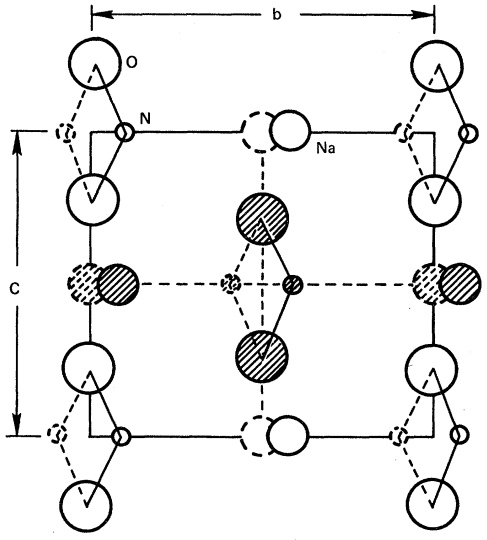


FIG. 1. Unit cells of $NaNO_2$. The atoms shown with the solid circles represent atomic positions in the ferroelectric phase ($C_{2V}^{20}$). The dashed circles correspond to the paraelectric phase ($D_{2h}^{25}$), where the nitrogen atom resides in two possible positions, the sodium atom is centered on the $b$ edge, and the oxygen atoms remain fixed. (Dimensional changes of the unit cell have been omitted.) The shaded atoms are in the plane, $\frac{1}{2}$ of a lattice spacing in the $a$ direction.

TABLE I. Temperature correlation chart.

| Expected change in Raman-active resonances $C_{2V}^{20}$ | $D_{2h}^{25}$ | Expected change in infrared-active resonances $C_{2V}^{20}$ | $D_{2h}^{25}$ |
|---|---|---|---|
| $3:A_1 \rightarrow 1:A_g$ ($aa$, $bb$, $cc$) | | $3\ A_1 \rightarrow 2\ B_{1u}$ | |
| $1:A_2 \rightarrow 1:B_{1g}$ ($ac$) | | $3\ B_1 \rightarrow 2\ B_{3u}$ | |
| $3:B_1 \rightarrow 1:B_{2g}$ ($bc$) | | $2\ B_2 \rightarrow 2\ B_{2u}$ | |
| $2:B_2 \rightarrow 0:B_{3g}$ (ab) | | 8 → 6 | |
| 9 → 3 | | | |

perature is above $T_N$. The correlation chart in Table I maps the symmetry elements of the $C_{2V}^{20}$ symmetry into the high $D_{2h}^{25}$ symmetry, showing the expected changes in the Raman scattering, while using the different Raman polarization filters [polarization orientations ($aa$), ($bc$), etc.]. The atomic motions corresponding to the various irreducible species are shown in Fig. 2.[27] The normal modes consist of three internal vibrations (movements of only the atoms in the $NO_2^-$ ion) and six external vibrations (movements of the nitrite ion and the sodium ion, as if they were point masses).

## III. EXPERIMENTAL TECHNIQUE

The frequencies and linewidths of the lattice modes of $NaNO_2$ were investigated using the Raman-scattering technique. The temperature dependency of the Raman-observable TO frequencies and linewidths was followed from 20 to 250 °C. The characteristic frequencies were chosen to represent peak heights of the scattering, and the linewidths, to represent the separation of the frequencies at the half-height intensities. (Linewidths were corrected for spectrometer broadening, and spectra with merged resonances were computer analyzed for linewidths and resonant frequencies.) Temperature-hysteresis effects were not included in the study; only data obtained from heating the crystal were used. The scattering configurations used to trace the different symmetry modes as a function of temperature are shown in Fig. 3. The propagation directions and polarizations of the incident light were such that birefringence could not produce ambiguous

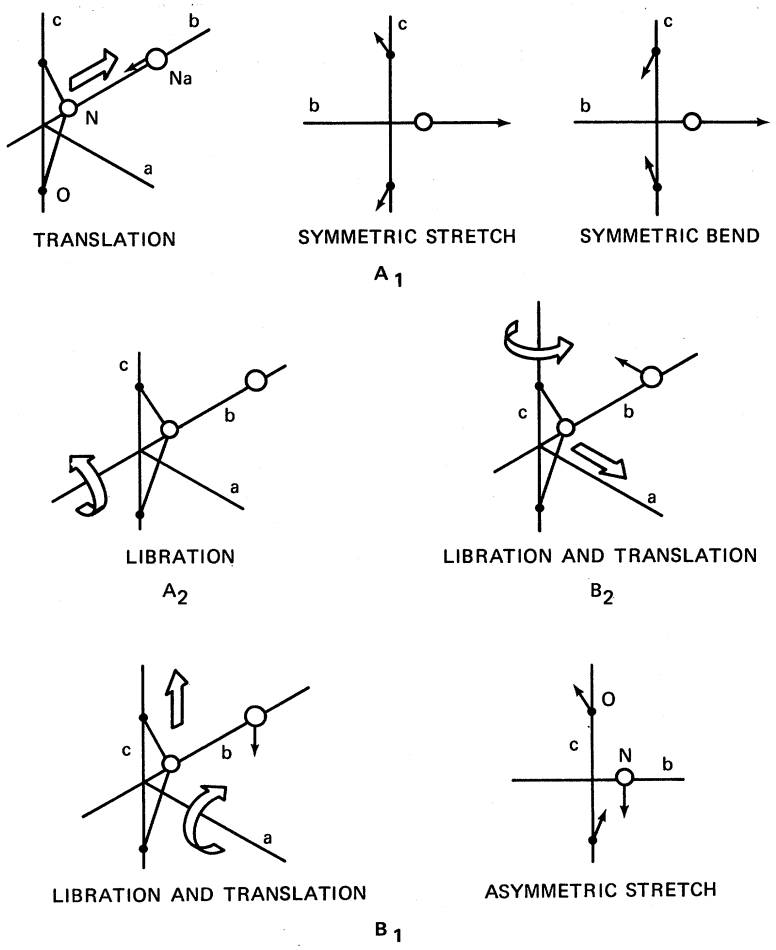


FIG. 2. Normal modes for ferroelectric $NaNO_2$. The vectorial arrows indicate only qualitativity, not quantitatively, atomic motions.

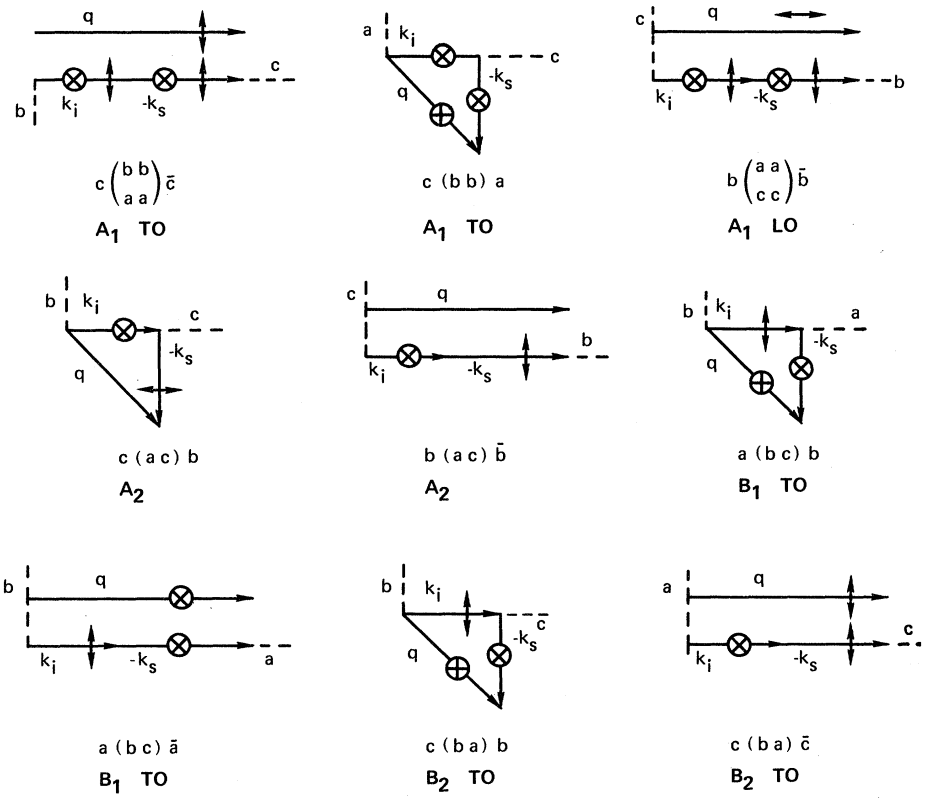


FIG. 3. Raman-scattering diagrams for $NaNO_2$. These scattering geometries will detect all the TO modes, the $A_1$ (LO) mode, and the $A_2$ mode. The small arrows give the directions of the electric and ionic polarizations.

results.

The TO modes of the $B_1$, $B_2$, and $A_1$ symmetry phonons and the $A_2$ nonpolar mode were seen in both backscattering and right-angle-scattering geometries, providing a check on their eigenfrequency invariance. The $A_1$ LO values were seen in both backscattering and right-angle geometries. Obtaining the LO frequencies of the $B_1$ and $B_2$ irreducible symmetry modes was not straightforward, such as the Raman tensors would seem to indicate. The frequency difference between the incident and Stokes scattered light and the biaxial nature of the crystal forced mismatches in wave-vector conservation ($\vec{K}_L = \vec{K}_S + \vec{K}_{\text{phonon}}$) that did not allow direct observations of the salient LO phonons. Only the "oblique" phonons could be detected, and they present a range of frequencies consistent with their angular dispersion. (The LO frequencies of the $B_1$ and $B_2$ symmetry phonons have been found by such angular dispersion measurements, as described in Ref. 16, which contains a thorough discussion of the "oblique"-phonon phenomena.) Because there was great difficulty in obtaining the LO frequencies, and because all of the useful phase-transition information should have been reflected in the TO-mode behavior, only the temperature behavior of the Raman-active TO modes was observed.

To look for a possible softening of an optical mode or anomalous collective mechanisms, the Raman spectra were extended to 3 $cm^{-1}$ off the laser line. An iodine filter,[28] which absorbs the single-moded 5145-Å laser line, reduced the background Rayleigh scattering by about 500, when slits 100 $\mu$ wide were used in the spectrometer. These proximity scans were run at temperatures both above and below the transition temperature.

The 5145- and 4880-Å lines of the CRL model No. 52 argon-ion laser were used to irradiate the crystal. The scattering light was collected and put into a Spex model No. 1401 double spectrometer, using an ITT 130 photomultiplier and conventional dc recording. A Marshall tubular furnace and Norton controller were used to stabilize temperatures across the crystal to within $\pm 0.75$ °C. No attempt was made to study the extremely narrow ferrielectric (antiferroelectric) phase between 163 and 164 °C because of this temperature resolution. The temperature was monitored by a chromel-alumel thermocouple, which was pressed against the crystal.

The crystals of $NaNO_2$ were grown from the melt. Anisotropic thermal-expansion coefficients[29] can cause cracking of the crystal, as it attaches to the crucible surface during temperature changes; therefore, the crystal was pulled out from the melt before it reached the walls and was immediately cleaved along the (101) and (10$\bar{1}$) planes.[30] Large single crystals with faces perpendicular to the crystallographic axes were then cut out and polished.

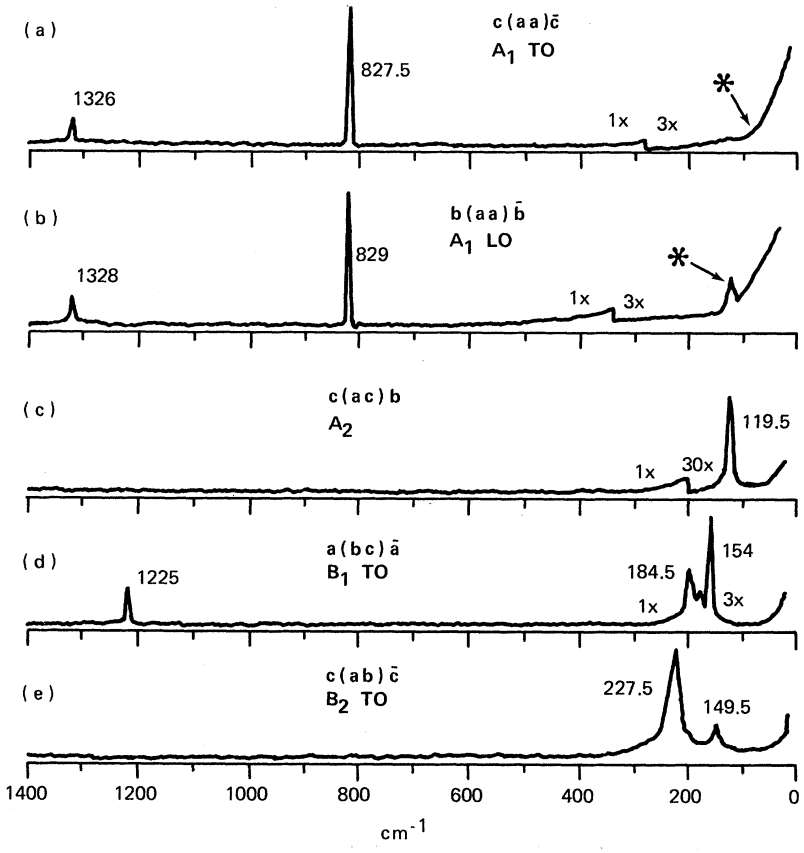


FIG. 4. Room-temperature Raman spectra from $NaNO_2$. The asterisk indicates orientational spillovers of scattering from the $A_2$ phonons. Intensity-scale changes are marked by 1×, etc.

Twinning perpendicular to the *ac* crystallographic plane[31] produced domains in these crystals. [The twinning merely introduces an inversion symmetry ($b \rightarrow -b$), which does not affect the polarization selection rules. Additionally, as the domains have dimensions much larger than the wavelengths of the radiation,[31] wave-vector conservation is also still applicable.] The orientations, checked with x rays, were to within ±1°. The orientational error of placement in the furnace was ±3°.

## IV. RESULTS

Spectra of the room-temperature Raman scattering from the TO and LO modes of $A_1$ symmetry, from the mode of $A_2$ symmetry, and from the TO modes of $B_1$ and $B_2$ symmetry, are shown in Fig. 4. The $A_2$ mode is very strong and appears in almost all of the spectra because of the large solid angle of the collecting optics. The Raman spectra of $NaNO_2$ in its ferroelectric phase show only seven of the eight TO-LO frequency pairs predicted to be Raman active from group-theory considerations. Neither the TO or the LO of the lowest frequency mode of the $A_1$ representation (194-$cm^{-1}$ TO frequency) could be directly detected. However, for the first time Raman spectroscopy was able to measure the LO frequencies of the modes of the $B_1$ and $B_2$ symmetry. The angular dispersion of mixed modes, "oblique phonons," was measured in the *ac* crystallographic plane by Raman scattering (Fig. 5).[32] As explained in our earlier publication,[16] this angular dispersion is accurately characterized by

$$\sum_{k=1}^{3} \alpha_k^2 \epsilon_{\infty k} \prod_{j=1}^{n^k} \frac{\omega_{jk}^2(\mathrm{LO}) - \omega_{\vec{q}}^2}{\omega_{jk}^2 - \omega_{\vec{q}}^2} = 0 \ , \tag{3}$$

where $\vec{q}$ is the phonon propagation direction, $\vec{n}_k$ is the unit vector parallel to $k$th crystallographic axis, $\alpha_k = \vec{q} \cdot \vec{n}_k / q$, $\epsilon_{\infty k}$ is the optical permittivity, $n^k$ is the number of modes with polarization parallel to the $k$th axis, $\omega_{jk}$ is the TO frequency of the $j$th mode, whose polarization is parallel to the $k$th axis, $\omega_{jk}(\mathrm{LO})$ is the LO frequency of the $j$th mode, where polarization is parallel to the $k$th axis, and $\omega_{\vec{q}}$ is the frequency of phonon propagating in the $\vec{q}/q$ direction.

The limiting frequencies of the angular dispersion occurring for phonon propagation directions along crystallographic axes are TO and LO values. Measured dispersion data in the *ac* crystallographic plane were fitted with Eq. (3) by adjusting the unknown LO frequencies of the $B_1$ and $B_2$ modes. Figure 5 shows the measured angular dispersion in the *ac* plane and the expected dispersion in the *ab* and *bc* planes (the TO and LO frequencies of the $A_1$ translation mode were taken from infrared data[11,14]).

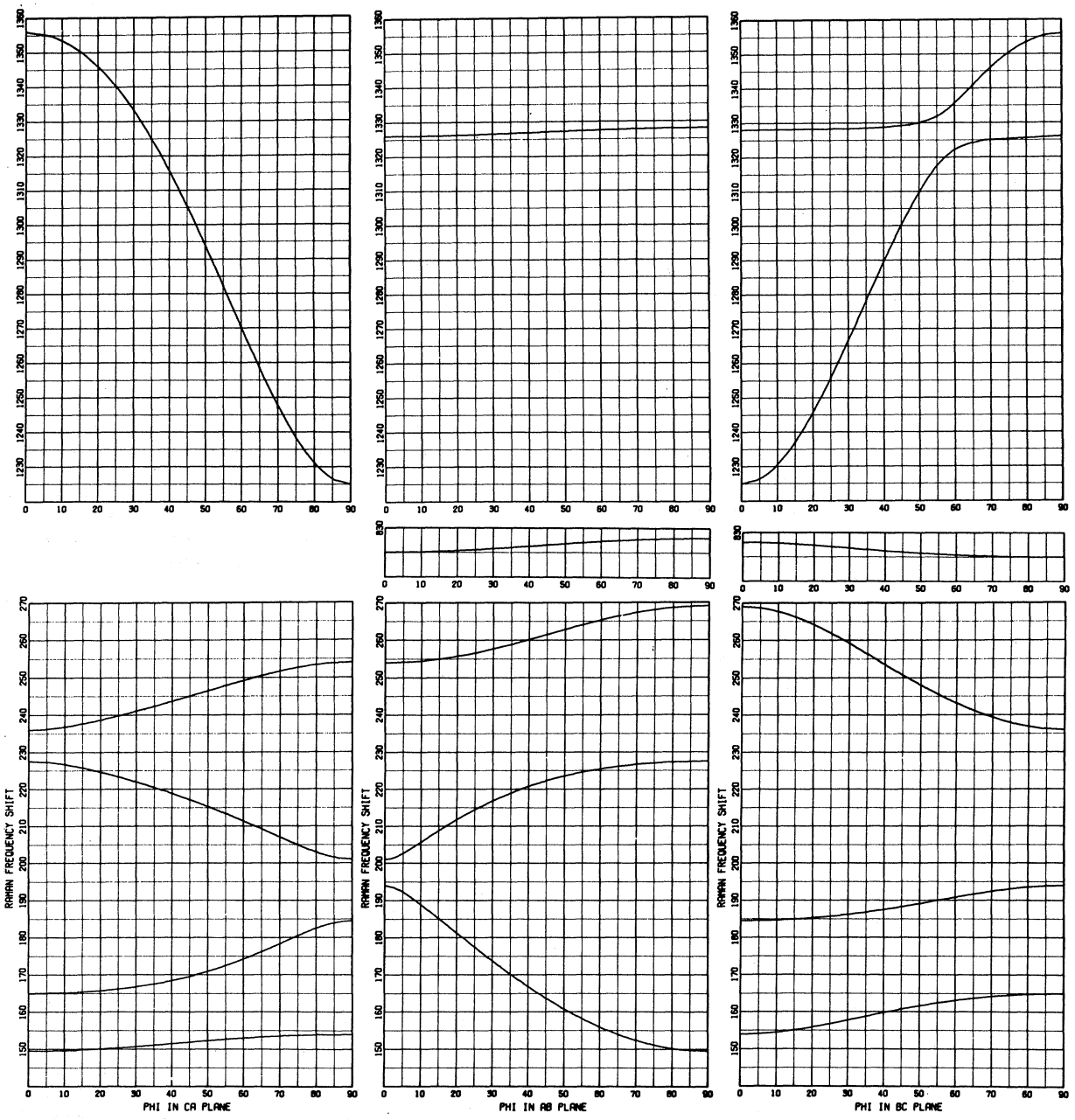


FIG. 5. Angular dispersion in $NaNO_2$ (Ref. 32). Phi is the angle between $\vec{q}$ and the $c$ axis, $\vec{q}$ and the $a$ axis, and $\vec{q}$ and the $b$ axis for phonon propagation in the $ca$, $ab$, and $bc$ crystallographic planes, respectively. The plot in the $ac$ plane has been experimentally confirmed (Ref. 16).

These uniquely determined LO frequencies, along with our other Raman-found TO and LO frequencies for the ferroelectric phase, are compared in Table II with previous infrared and Raman results.

The effects of heating upon the frequencies and linewidths of the Raman-observable modes in $NaNO_2$ are shown in Fig. 6 (the internal modes) and Fig. 7 (external modes). Surprisingly, the data show that six of the eight observed lines (instead of the expected three) retain sufficient scattering strength to be seen in the paraelectric phase. The two modes that disappear [labeled $B_1$ (translation) and $B_2$ (translation)] exhibit a gradual decrease of scattering strength and merge into adjacent modes, as the transition temperature is approached (Figs. 7 and 8). All lines, except the eigenfrequencies of the $A_2$ (libration), are affected by the phase transition. The temperature history of the line that is

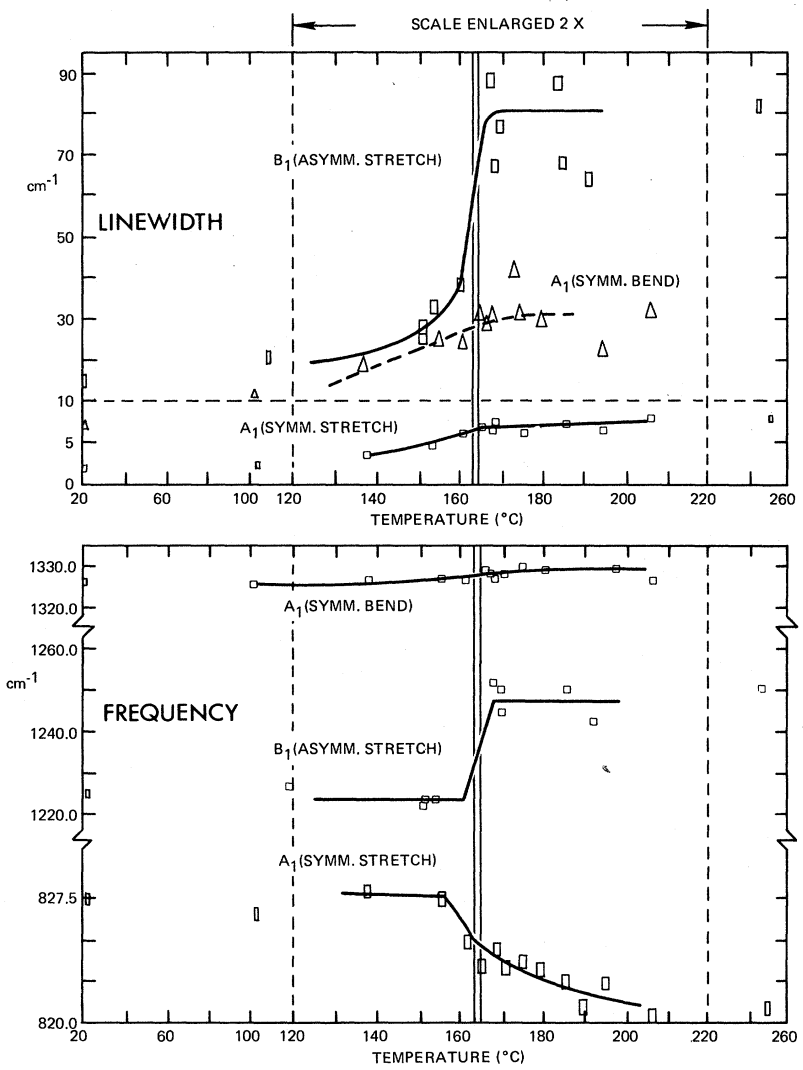


FIG. 6. Frequencies and linewidths of the Raman resonances in the internal-frequency spectra as a function of temperature. The phase transition occurs between the solid vertical lines. The nomenclature for the resonances refers to their character in the ferroelectric phase.

TABLE II. Resonant frequencies ($cm^{-1}$), dielectric transition strengths, and static permitivities in $NaNO_2$ at room temperature. The full linewidths at half-peak intensity are included for the TO lines and labeled $\gamma_{TO}$ (the damping constant).

| | Infrared | | | | Raman | | | | Raman | | | Dielectric transition strengths[a] |
|---|---|---|---|---|---|---|---|---|---|---|---|---|
| | Ref. 11 | | Ref. 14 | | Ref. 17 | | Ref. 15 | | | | | |
| | TO | LO | TO | LO | TO | LO | TO | LO | TO | LO | $\gamma_{TO}$ | $S_j k$ |
| | 194 | 269 | 186.8 | ••• | ••• | ••• | ••• | ••• | ••• | ••• | ••• | 2.085[b] |
| $A_1$ | 826 | 829 | 825.3 | ••• | 825 | ••• | 830 | ••• | 827.5 | 829 | 1.5 | 0.0715[b] |
| | 1323 | 1336 | 1320.5 | ••• | 1327 | ••• | 1323 | ••• | 1326 | 1328 | 7.5 | 0.0041[b] |
| $A_2$ | ••• | ••• | ••• | ••• | 119 | ••• | 117 | ••• | 119.5 | ••• | 10 | 0.000 |
| | 157 | 163 | 150.9 | ••• | 153 | ••• | 158 | ••• | 154 | 165 | 8 | 1.519 |
| $B_1$ | 188 | 250 | 180.7 | ••• | 177 | ••• | 191 | ••• | 184.5 | 236 | 15 | 1.420 |
| | 1235 | 1368 | 1227.3 | ••• | 1280 | ••• | 1230 | ••• | 1225 | 1356 | 14 | 0.608 |
| | 149 | 193 | 145.7 | ••• | ••• | ••• | ••• | ••• | 149.5 | 201 | 16 | 2.085 |
| $B_2$ | 223 | 261 | 231.7 | ••• | 220 | ••• | 223 | ••• | 227.5 | 254 | 25 | 0.178 |
| | $\epsilon_0^a = 4.10$ | | $\epsilon_0^b = 4.20$[b] | | $\epsilon_0^c = 6.27$ | | | | | | | |

[a]Calculation was made with Eq. (5) from Ref. 16, using the values of this work.
[b]Calculation uses the three LO and TO frequencies of the external mode (194-TO) from Ref. 11.

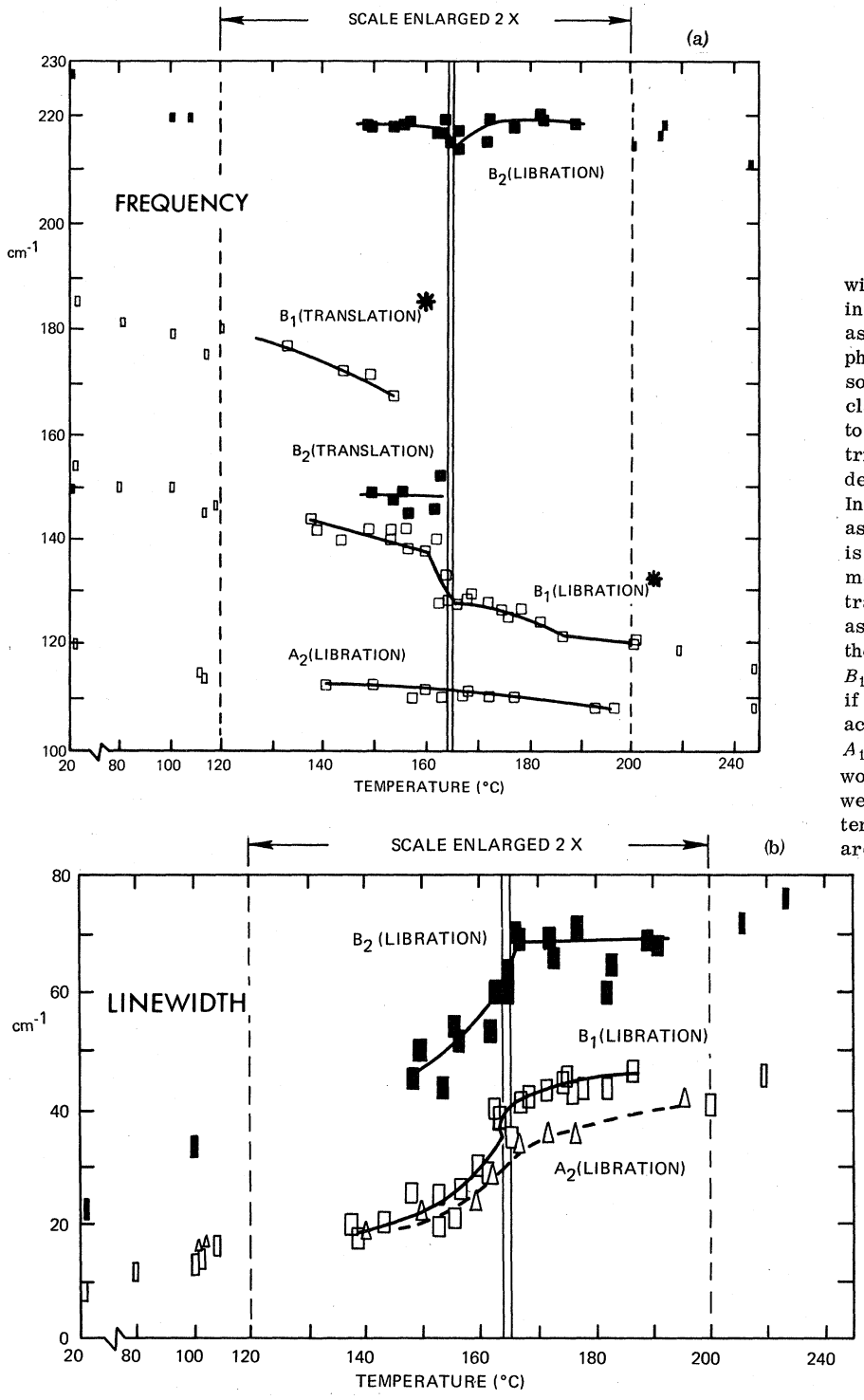


FIG. 7. Frequencies and linewidths of the Raman resonances in the external-frequency spectra as a function of temperature. The phase transition occurs between the solid vertical lines. The nomenclature for the resonances refers to their character in the ferroelectric phase. (a) The temperature-dependent frequencies are shown. In the ferro-electric phase the line assignment marked by the asterisk is contrary to the historical assignment of the highest frequency of a translational-librational ambiguity as a libration. It is believed that the paraelectric assignment of the $B_1$ (libration) is correct, so that if the conventional assignment were accepted, a cross-over between the $A_1$ (translation) and $B_1$ (libration) would have to occur, which is a fact we could not determine. (b) The temperature-dependent linewidths are shown.

identified as the libration about the $a$ axis of the $B_1$ irreducible species is of special interest. This state's TO frequency definitively softens near two critical temperatures, the phase-transition temperature and 178 °C, a temperature that has been suggested by Hoshino and Shibuya[29] and Takagi and Gesi[33] as delineating the onset of the short-range order loss in sodium nitrite. These softenings must accompany a decrease of the potential hill separating the two orientational states of the nitrite ion in this rotational coordinate. Once softened, this frequency [$B_1$ (libration)] remains at its lower

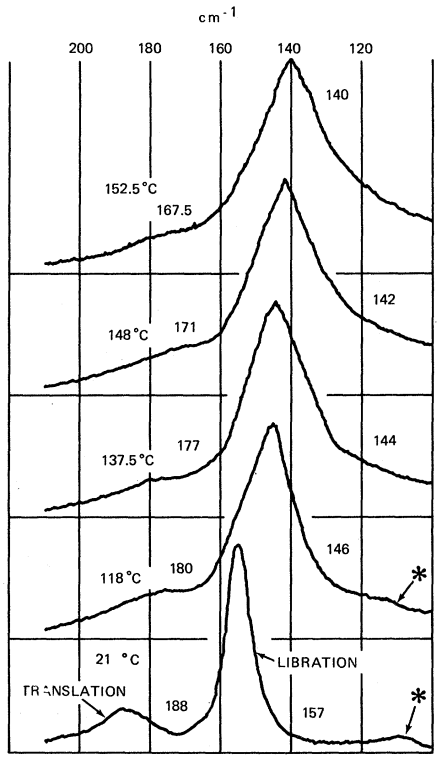


FIG. 8. Raman scattering from the $B_1$ phonons (libration about the $a$ axis and translation along the $c$ axis) as a function of temperature. The asterisk indicates orientational spillover of scattering from the $A_2$ phonons. At higher temperatures this scattering, plus the temperature-enhanced Rayleigh scattering, contributes to the large scattering intensity seen on the low-frequency side of the libration.

value throughout the paraelectric phase, in contrast to the frequency of the $B_2$ (libration) (Fig. 7).

Figures 8 and 9 present the temperature dependency of the line shapes of three of the Raman-observable resonances. Figure 8 shows the line-shape changes of the modes, which are assigned the character of the libration about the $a$ axis and the translation along the $c$ axis, two modes whose irreducible species are the same in the ferroelectric phase. An important observation about this data is the increasing overlapping of these two lines as the phase-transition temperature is approached (temperature-dependent reflection data exhibit similar overlapping[14]). The high-frequency resonance in Fig. 5, in addition to being absorped by the lower-frequency resonance, exhibits an integrated scattering decrease as the temperature increases; it becomes undetectable shortly before $T_c$. This is also true of the resonance labeled $B_2$ (translation) in Fig. 7. In Fig. 9, the temperature dependency of the lattice states of the symmetric stretch is shown. The characteristic asymmetry that appears in the paraelectric phase for this mode is seen for all the internal modes.

As stated previously, only three distinct lines were expected to be seen with the various Raman filters in the paraelectric phase. Figure 10 shows typical Raman spectra of the paraelectric phases and Table III lists the Raman-distinguishable frequencies in the paraelectric phase. These data show an anomalous appearance of six, rather than three, characteristic frequencies. The second striking anomaly in the spectra is the detectability of the symmetric stretch (821 $cm^{-1}$) and the symmetric bend (1328 $cm^{-1}$) in the depolarized ($bc$) spectra, as well as in the anticipated polarized spectra.

## V. DISCUSSION

The discussion of the Raman data is divided into three parts, commensurate with the crystalline temperature regimes in the crystal: the ferroelectric phase, the paraelectric phase, and the phase transition.

### A. Ferroelectric Phase

Interpretation of our Raman data from $NaNO_2$ is only in agreement with the group-theoretical predictions based on $C_{2v}^{20}$ space-group symmetry with one molecule per unit cell, thus confirming its use with sodium nitrite (Table II). The absence of the

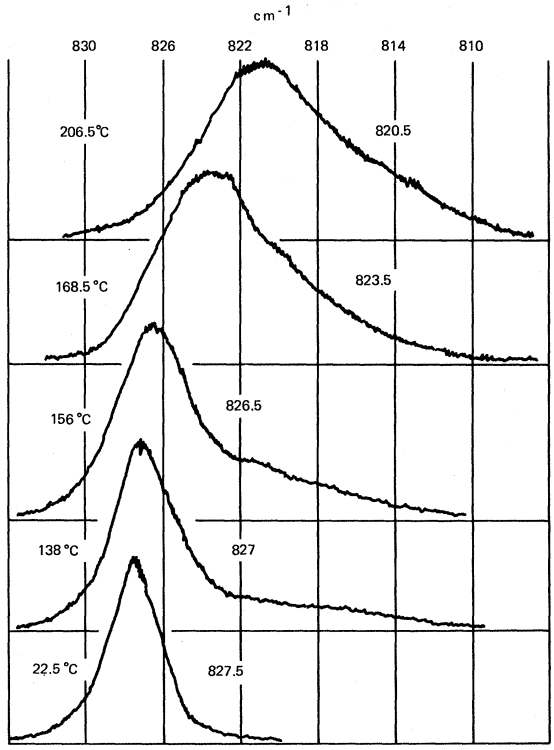


FIG. 9. Raman scattering from the symmetric stretch as a function of temperature.

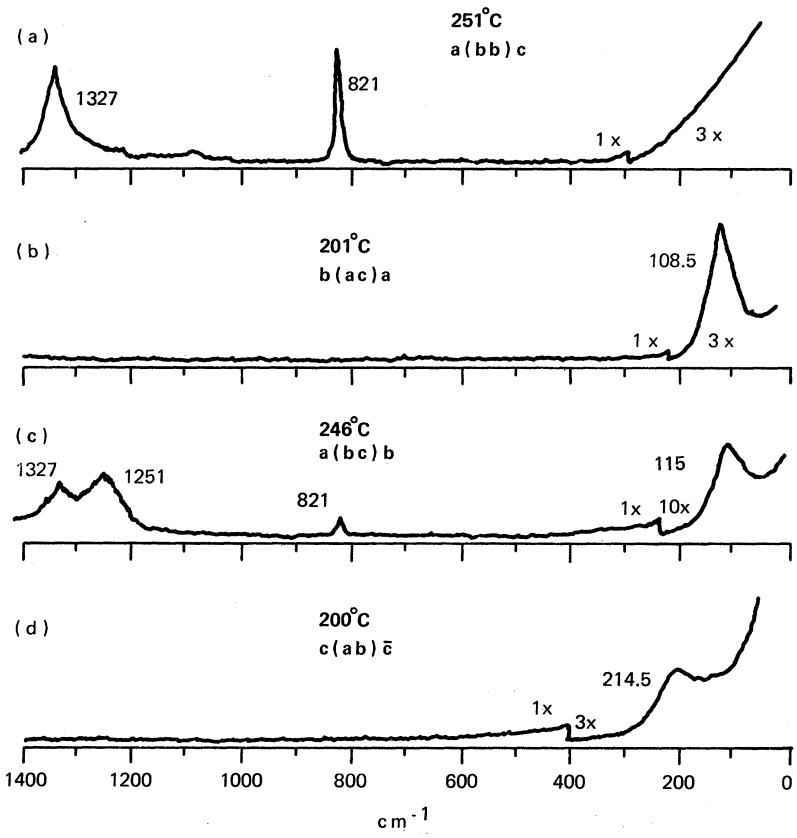


FIG. 10. Raman spectra from $NaNO_2$ in the paraelectric phase. Intensity-scale changes are marked by 1×, etc. The intensity increase at the low-frequency end of the spectra is due to Rayleigh scattering.

lowest-frequency $A_1$ symmetry mode (TO 194 $cm^{-1}$, as seen in infrared observations[11,14]) from Raman detection does not contradict this conclusion. Its absence in the Raman spectra simply implies a very weak Raman coupling. A unique aspect of our experimental data is the LO frequencies of the $B_1$ and $B_2$ modes, which were found by the indirect observation of the angular-dispersion curves. These angular-dispersion measurements point out, by the way, that in evaluating Raman or infrared spectra from anisotropic crystals, one must be cognizant of the scattered-phonon propagation direction. In essence, a new symmetry element is introduced for a crystal when an infrared-active mode propagates along other than a crystallographic direction; this spoils the applicability of the selection rules based on a static crystal structure (see Ref. 16 for a more complete discussion). Also presented in Table II are the static permittivities $\epsilon_0^k$; ignoring damping, they are calculated from the generalized Lyddane-Sachs-Teller (LST) relation[34] or from the induced dielectric strengths $S_j^k$,[16]

$$\frac{\epsilon_0^k}{\epsilon_\infty^k} = \prod_{j=1}^{n^k}\left(\frac{\omega_j^k(\mathrm{LO})}{\omega_{jk}}\right)^2 = 1 + \sum_{j=1}^{n^k} S_j^k \Big/ \epsilon_\infty^k \,. \qquad (4)$$

The values of the dielectric constants determined from our Raman-spectral data are lower than those reported in the MHz region,[35] but they are in agreement with the values determined from the infrared measurements.[11,14]

### B. Paraelectric Phase

Raman spectra for sodium nitrite in the paraelectric phase, based on the $D_{2h}^{25}$ space-group symmetry with one molecule per unit cell, was predicted to be easily interpretable with only three resonances. The understanding of our Raman data, however, was complicated by the appearance of extra resonances, asymmetric line shapes, and the redundant appearance of internal resonances.

In accordance with group-theoretical calculations for the average $D_{2h}^{25}$ space-group symmetry of the disordered phase of sodium nitrite, only three

TABLE III. Raman-observed frequencies in the paraelectric phase of $NaNO_2$ at around 200 °C.

| Irreducible species | Second-rank tensor | Raman-observed frequencies ($cm^{-1}$) | | | |
|---|---|---|---|---|---|
| $A_g$ | *aa*, *bb*, *cc* | | 821 | | 1328 |
| $B_{1g}$ | *ac* | 108 | | | |
| $B_{2g}$ | *bc* | 120.5 | 821 | 1251 | 1328 |
| $B_{3g}$ | *ab* | 215 | | | |

resonances were to remain Raman active at temperatures above $T_N$. After extensive reexamination, however, we concluded that there were six, not three, distinguishable frequencies in our Raman spectra (Table III). We have reevaluated the use of the $D_{2h}^{25}$ space symmetry group for the Raman-selection-rule determination and have concluded that the reason for the superfluity of the Raman-detectable lines is the misuse of the x-ray-determined crystalline symmetry to describe the Raman scattering. X-ray scattering measurements are time averaged and include scattering from the entire specimen. Although x-ray spectroscopists are aware of disorder through diffuse scattering, this average scattering is insensitive to the temporal and spatial disordering occurring in microdomains within the sample. It is just this average scattering that is matched by the $D_{2h}^{25}$ symmetry group. Raman and infrared spectroscopy, however, sample across a disorded microdomain. Because these processes interact at time rates faster than the expected flipping rate of the disordering ($10^{-13}$ sec compared to $10^{-11}$ sec),[36] Raman and infrared spectroscopy can instantaneously observe these disordered microdomains. The disordered instantaneous microdomain has no real center of inversion, and, hence, all the modes that are affected by this disordering will be both Raman and infrared active.[37]

The appearance of (i) the two internal frequencies (821 and 1328 $cm^{-1}$) instead of one in the polarized spectra, (ii) the internal frequency (1251 $cm^{-1}$) in the ($bc$) spectra, and (iii) the libration about the $c$ axis (215 $cm^{-1}$) in the ($ab$) spectra (Fig. 10) may thus be explained by the nitrite-ion disordering. In fact, the normal modes of the $D_{2h}^{25}$ space-group symmetry do not even include the libration about the $c$ axis. With the $D_{2h}^{25}$ space group, the $NO_2^-$ ion has to be depicted as linear along the $c$ axis to match the average x-ray scattering, thus exluding the libration about the $c$ axis as a mode possibility. The frequencies of 1251 and 215 $cm^{-1}$ were not to be seen in the paraelectric phase; they account for two of the additional unexpected resonances. The third additional resonance is either 821 or 1328 $cm^{-1}$. One of these resonances, unidentified by the $D_{2h}^{25}$ selection rules, was predicted to be only Raman active. As we had argued, however, all six of these modes are Raman and infrared active.

The translational frequencies with polarizations parallel to $c$ and $a$, respectively, move the $NO_2^-$ ion as a point and will be relatively unaffected by the $NO_2$-ion disordering. Thus they closely conform to the lattice selection rules based on $D_{2h}^{25}$ symmetry and, hence, are not seen in the Raman spectra of the paraelectric phase, disappearing in our data as the transition temperature is approached. In fact, it is within this logic that we have identified the librational and translational peaks (Figs. 4, 5, and 7). In the temperature-dependent Raman spectra the disappearing external modes are identified as the translational modes (Fig. 8).

The second anomaly in our Raman spectra was the curious line shapes that appeared in the paraelectric phase (Fig. 10). Both Stokes and anti-Stokes spectra displayed these peculiar line shapes. Here again the disordering inherent in this paraelectric phase generates a spectral anomaly. Within a disordered microdomain there is a loss of translational symmetry, and subsequently the sampling of phonons with only very small wave vectors is not mandatory upon the Raman process; wave-vector conservation is not obeyed. The spectra are a function of a multiplication of all possible resonant frequencies, with the corresponding frequency-dependent densities of states.[37] Thus, normal Lorentzian lines should not be expected and do not appear, as witnessed by our Raman observations.

The remaining confusion in the Raman spectra is the appearance of the 821 and the 1328 $cm^{-1}$ frequencies, two frequencies of the internal vibrations, in both the polarized and depolarized ($bc$) spectra (Fig. 10). Neither nitrite-ion disordering or experimental error explains this spectral doubling. What does explain this spectral redundance is a large oscillation of the $NO_2^-$ radical about the $a$ axis; the occurrence of this oscillation has been intimated by Sato *et al.*[12] and by Chisler and Shur.[17] With a large misalignment of the bisecting axis of the O–N–O angle with the $b$ axis, such that the nitrogen and oxygen atoms are moving in the $bc$ crystallographic plane, the lattice modes involving the symmetric bend and symmetric stretch in the $NO_2^-$ ion have irreducible species described by both symmetric and $bc$ basis functions; hence, these lines can be seen with polarized and ($bc$) Raman filters. If the large torsional oscillation were not present, the internal vibrations would appear only in the polarized spectra. Movement about any other axis would necessitate the appearance of the symmetric vibrations and of the asymmetric vibration in other depolarized spectra.

### C. Order-Disorder Phase Transition

The complicated two-stage phase transition in $NaNO_2$ is an intriguing puzzle, which we had hoped to unravel with Raman spectroscopy. We have found that our Raman data give no support to transition mechanisms involving a soft mode, dipole wave, or tunneling. However, the data do suggest a mechanistic possibility that could explain the means of the nitrite-ion disordering and its ability to participate in the phase transition.

There is no evidence in our experimental results of "Cochran" soft modes to precipitate the order-disorder phase transition. The temperature profiles of the TO frequencies (Fig. 7) show no modes

going to zero frequency as the ambient temperature of the crystal is raised to the ferroelectric demarcation. On the basis of infrared experiments[13,14] the translational mode not observed in the Raman spectra also shows no indication of this critical soft-mode behavior; thus, a "Cochran" soft mode cannot account for the loss of the ferroelectricity in $NaNO_2$.

Within the content of our Raman data we also eliminate two other phase-transition possibilities. Extending our measurements in the $c(ba)\bar{c}$, $b(ca+b)c$, and $b(ab+a)c$ scattering configurations to 3 $cm^{-1}$ away from the exciting laser frequency revealed only a featureless background, which showed no change as the crystal approached the phase transition, except for increased Rayleigh scattering. Thus, there is also no evidence from Raman spectroscopy of any low-frequency dipole wave greater than 3 $cm^{-1}$, functioning along the polar axis of sodium nitrite. Concomitantly, the lack of a low-frequency scattering peak in the Raman spectra and the absence of frequency-doubling evidence in the Raman spectra of the paraelectric phase (resolution 1 $cm^{-1}$) imply that there is no rotational- or translational-tunneling mechanism operable at frequencies greater than 3 $cm^{-1}$. (Sato *et al.*[12] also conclude that there is no tunneling of the nitrogen atom between the oxygen atoms.)

We do believe, however, that there is strong evidence in our Raman data of a mechanism that disorders the nitrogen atom about the *ac* plane. In our discussion of the paraelectric phase, we noted the ambiguous appearance of the internal vibrations in the polarized and $(bc)$ Raman spectra of the paraelectric phase, which was accounted for by a large torsional oscillation of the $NO_2^-$ ion about the $a$ axis (Fig. 10). Additionally, in our discussion of the temperature profiles of the normal modes' TO frequencies, we pointed out the observed softening of the characteristic frequencies of the libration about the $a$ axis at the fundamental temperatures, at which long-range and short-range orders are lost (Fig. 7). From these two observations, we conclude that in the paraelectric phase the temperature-dependent lattice dynamics relax their restraints on the rotation of the $NO_2^-$ ion about the $a$ axis, and that this rotation can then flip the $NO_2^-$ ion. Thus the disordering mechanism for the nitrogen atom is this flipping about the $a$ axis of the nitrite ion. Incidently, we have found no evidence to indicate that the $NO_2^-$-ion disordering is caused by the apparently easier mechanism, a rotation about the $c$ axis. This flipping of the $NO_2^-$ ion about the $a$ axis, as it determines the state of order in the crystal, is a critical parameter in determining the onset of the phase transition.

We are still plagued with a fundamental question: Given that the rotation about the $a$ axis of the nitrite ion and the centering of the $Na^+$ atom on the $b$ axis of the unit cell are two critical parameters that determine the phase transition in $NaNO_2$, how are they affected by the ambient temperature, such that they are able to initiate the phase changes at $T_c$ and $T_N$? We here make a suggestion, based upon our Raman data, which will deal with the temperature-dependent tendency of the nitrite ion to flip.

Earlier, we discussed the increasing overlapping of the translational and librational modes of $B_1$ irreducible species (translation parallel to $c$ and libration about $a$) in the ferroelectric phase, as the transition temperature was approached (Figs. 7 and 8). We now conjecture that the merging of these two normal modes' lattice states in their band edges permits energy exchange between them. This crystalline vibrational coupling has a simple analogy in the coupling between a vibrational and a torsional oscillator in classical mechanics (an example is the Wilberforce oscillator[38]). Just as energy is fed between the torsional and vibrational oscillators in the classical situation (the energy exchange occurs at a lower frequency than the normal frequencies of the oscillators), so now energy may be exchanged between the translation and librational phonon states in a crystal. As the temperature increases in the ferroelectric phase, the observed spectral overlapping increases (the resonant frequencies remain separated by about the same energy), hence, the coupling between the oscillators increases. The torsional oscillation of the $NO_2^-$ anion about the $a$ axis then also increases. At the phase-transition temperature, the thermodynamic potential of the crystal will be minimized by a new set of crystalline parameters, which will include the centering of the $Na^+$ ion on the $b$ axis and the disordering of the nitrogen atom, which has been prepared by the temperature-augmented torsional oscillation due to lattice-mode coupling and the rotational potential barrier decrease as discussed earlier. In the paraelectric phase, flipping of the $NO_2^-$ ion will now occur through this coupled oscillator mechanism. (The flipping frequency of the nitrite dipole is thought to be about $10^{11}$ cps,[36] while the normal mode frequencies are about $450\times10^{10}$ cps.) The culminating action in the $NO_2^-$ flipping may be a tunneling through the rotational potential hill or a free rotation over the barrier. [It is possible that the internal asymmetric vibration, which shows frequency and linewidth anomalies at the phase connection temperature (Fig. 6), may also participate in this flipping.] This suggestion warrants further experimentation and analytical evaluation, with which two of the authors, Wiener-Avnear and Porto, are proceeding. It may well also contribute to the explanation of other phase transitions.

## VI. SUMMARY

Raman-scattering experiments from $NaNO_2$ single

crystals at room temperature confirm the selection-rule predictions for the ferroelectric phase and account for the static dielectric constants along the three major axes. Raman spectra of the disordered phase in sodium nitrite reveal selection-rule violations and line-shape asymmetry that are explained by the instantaneous disordering in the crystal and by a large torsional oscillation of the nitrite ion about the $a$ axis. Temperature-dependent scattered intensities are used to identify the ambiguous librations and translations. We further propose that the nitrogen-atom disordering is produced by a flipping of the nitrite anion about the $a$ axis, whose oscillating strength may be dependent upon a temperature-dependent coupling between the translation parallel to the $c$ axis and the libration about the $a$ axis.


## ACKNOWLEDGMENTS

We thank Professor J. Smit of the University of Southern California for his generous aid and penetrating discussion, and E. H. Barsis of Sandia Laboratories (Livermore, California) and D. L. Rousseau of Bell Telephone Laboratories for their edifying comments on this paper.


---

*Work sponsored by NSF Grant.

†Present address: Sandia Corporation, Livermore, Calif. 94550.

‡Present address: Physics Department, The University of the Negev, Beer-Sheva, Israel.

[1]M. Di Domenico, Jr., S. H. Wemple, S. P. S. Porto, and R. P. Bauman, Phys. Rev. 174, 522 (1968); L. Rimai, J. L. Parsons, J. T. Hickmott, and T. Nakamura, *ibid.* 168, 623 (1968).

[2]P. A. Fleury, J. F. Scott, and J. M. Worlock, Phys. Rev. Letters 21, 16 (1968).

[3]W. Cochran, Phys. Rev. Letters 3, 412 (1959); Advan. Phys. 9, 387 (1960).

[4]S. Sawada, S. Nomura, S. Fujii, and I. Yoshida, Phys. Rev. Letters 1, 320 (1958).

[5]I. Shibuya, J. Phys. Soc. Japan 16, 490 (1961).

[6]K. Gesi, J. Phys. Soc. Japan 20, 1764 (1965).

[7]S. Sawada, S. Nomura, and Y. Asao, J. Phys. Soc. Japan 16, 2207 (1961).

[8]S. Nomura, J. Phys. Soc. Japan 16, 2440 (1961).

[9]Y. Takagi and K. Gesi, J. Phys. Soc. Japan 22, 979 (1967).

[10]I. Hatta, J. Phys. Soc. Japan 24, 1043 (1967).

[11]J. D. Axe, Phys. Rev. 167, 523 (1968).

[12]Y. Sato, K. Gesi, and Y. Takagi, J. Phys. Soc. Japan 16, 2172 (1961).

[13]H. Vogt and H. Happ, Phys. Status Solidi 16, 711 (1966); 30, 67 (1968).

[14]M. K. Barnoski and J. M. Ballantyne, Phys. Rev. 174, 946 (1968).

[15]M. Tsuboi, M. Terada, and T. Kajiura, Bull. Chem. Soc. Japan 41, 2545 (1968); 42, 1871 (1969).

[16]C. M. Hartwig, E. Wiener-Avnear, J. Smit, and S. P. S. Porto, Phys. Rev. B 3, 2078 (1971).

[17]E. V. Chisler and M. S. Shur, Phys. Status Solidi 17, 163 (1966); 17, 173 (1966); Fiz. Tverd. Tela 9, 1015 (1967) [Sov. Phys. Solid State 9, 796 (1967)]; Acad. Sci. USSR, Bull. Phys. Ser. 31, 1110 (1967).

[18]V. S. Gorelik, I. S. Zheludev, and M. M. Suschinskii, Kristallografiya 11, 604 (1966) [Sov. Phys. Crist. 11, 527 (1967)].

[19]G. E. Ziegler, Phys. Rev. 38, 1040 (1931).

[20]B. Strijk and C. H. MacGillavry, Rec. Trav. Chim. 62, 705 (1943); 65, 127 (1946).

[21]G. B. Carpenter, Acta Cryst. 5, 132 (1952).

[22]S. Taniskai, J. Phys. Soc. Japan 16, 579 (1961); 18, 1181 (1963).

[23]Y. Yamada, I. Shibuya, and S. Hoshino, J. Phys. Soc. Japan 18, 1594 (1963).

[24]S. Hoshino, J. Phys. Soc. Japan 19, 140 (1964).

[25]R. Loudon, Advan. Phys. 13, 423 (1964).

[26]E. B. Wilson, Jr., J. C. Decius, and P. C. Cross, *Molecular Vibrations* (McGraw-Hill, New York, 1955).

[27]G. Herzberg, *Infrared and Raman Structure* (Van Nostrand, Princeton, New Jersey, 1968).

[28]The use of $I_2$ as a filter was first suggested by L. L. Chase, S. S. Davis, G. E. Devlin, and S. Geschwird of Bell Telephone Laboratories.

[29]S. Hoshino and I. Shibuya, J. Phys. Soc. Japan 16, 1254 (1961).

[30]This crystal-growth procedure was suggested to us by M. K. Barnoski of Hughes Research Laboratories, Malibu, Calif.

[31]S. Nomura, Y. Asao, and S. Sawada, J. Phys. Soc. Japan 16, 917 (1961).

[32]The calculated dispersion curves were done by Prasab A. D. Rao of the University of Southern California, Los Angeles, Calif.

[33]Y. Takagi and K. Gesi, J. Phys. Soc. Japan 19, 142 (1964).

[34]A. S. Barker, Phys. Rev. 136, A1290 (1964).

[35]E. Nakamura, J. Phys. Soc. Japan 17, 961 (1962).

[36]Y. Yamada, Y. Fujii, and I. Hatta, J. Phys. Soc. Japan 24, 1053 (1968).

[37]E. Whalley and J. E. Bertie, J. Chem. Phys. 46, 1264 (1967); 46, 1271 (1967).

[38]R. H. Cannon, Jr., *Dynamics of Physical Systems* (McGraw-Hill, New York, 1967), p. 440.